

Electron Lifetime and Purity Monitor for the ICARUS T600 Detector

F. Arneodo^a, E. Bernardini^a, F. Cavanna^b, I. De Mitri^c,
A. Ferella^b, A. Haag^b, D. Mazza^b,
O. Palamara^a, G.B. Piano Mortari^b, E. Tatananni^a

November 21, 2002

^a INFN - Lab. Naz. del Gran Sasso, Assergi (Italy)

^b Dip. di Fisica Univ. dell'Aquila e INFN, L'Aquila (Italy)

^c Dip. di Fisica Univ. di Lecce e INFN, Lecce (Italy)

Abstract

A series of four technical notes are being made available about the Purity Monitor System for the ICARUS T600 detector. The present one is the first of this series and is dedicated to a general overview of the Purity Monitor working principles and of its technical design and realization. It contains also a summary about the applied method for the experimental evaluation of the electron lifetime and related error.

The second accompanying note refers to the general layout of the Purity Monitoring System in view of the installation of the T600 at the Gran Sasso Laboratory. The other two notes, in preparation, report respectively on the lifetime measurement during the Pavia test run with the first T600 half-module and on the read-out electronics performance.

1 The LAr purity and the electron lifetime

A fundamental requirement of the ICARUS technology is that electrons produced by ionizing particles might travel unperturbed in liquid Argon from the point of production to the collecting wire planes. To this extent, the presence of any electro-negative impurity diluted in the liquid must be reduced at extraordinarily low levels. Moreover, the purity must be preserved at all time during the detector operation in order to ensure stable performance.

The electron attachment to a generic electro-negative impurity of type S , diluted in the liquid, is characterized by two parameters [1]: the attachment rate K_S and the concentration ρ_S . If a number $N_e(0)$ of electrons are produced in LAr at time $t = 0$, we expect to find a reduced number of electrons at time t , according to

$$N_e(t) = N_e(0) e^{-t/\tau_e} \quad (1)$$

where τ_e is the "electron lifetime", related to the impurity parameters by

$$\tau_e = \frac{1}{K_S N_S} \quad (2)$$

The rate K_S is a function of the applied electric field. However, in the range from few tens to few hundreds of V/cm, usually employed in our applications, the rate can be assumed to be constant to a good approximation.

Industrial Argon contains, for instance, Oxygen at the level of $\rho(O_2) \sim 1\text{ppm}$. Oxygen molecules have high electron attachment rate, and this contamination is enough to impair the detector capabilities. Therefore the liquid has to be purified during the detector filling and preserved during the entire lifetime of the experiment.

It is evident that the LAr purity level must be precisely monitored in the various phases of the detector operation (LAr filling and running).

A dedicated device, the so-called Purity Monitor (PrM) was first developed [2] in 1989 by the ICARUS Collaboration. Successively, several PrM units have been assembled and extensively used with the various ICARUS prototypes.

2 Working principle of the Purity Monitor

The PrM working scheme is rather simple: it consists of a small double-gridded drift chamber immersed in the LAr volume of the detector and located outside the imaging volume boundaries. Bunches of electrons can be extracted from the cathode via photo-electric effect. The electron bunch moves toward the anode along the electric field lines, crossing a drift region between two parallel, transparent grids. During the drift time attachment to impurities may take place, reducing the amount of electron charge collected by the anode, compared to the charge extracted. The ratio of these charges is a function of the electron lifetime in LAr (τ_e) that can therefore be estimated. The lifetime is directly connected to the impurity concentration $N(O_2)$, the total concentration of impurities equivalent to Oxygen contaminant, by the inverse linear relationship of Eq. 2. The lifetime estimation thus provides a direct measurement of the LAr impurity content.

3 The PrM unit for the T600 detector

In view of the realization of the PrM units to be installed in the T600 module, the working principle has been retained, while the design has been revised [3]. The major modifications concern the mechanics, the signal read-out system and the choice of the photo-cathode material and of the light source. Each half-module of the T600 detector hosts six PrM units realized according to the scheme described in the following.

3.1 Mechanics and electrical connections

The PrM drift chamber consists of four parallel, coaxial electrodes [the (photo-)cathode disk K, a first grid GK at short distance from the cathode, a second grid GA facing the anode and the anode disk A at short distance from GA] and of a field-shaping system for the drift volume [formed by an array of 15 coaxial rings between GK and GA]. All these elements are in stainless steel. The layout of the PrM unit is schematically reported in Fig. 1.

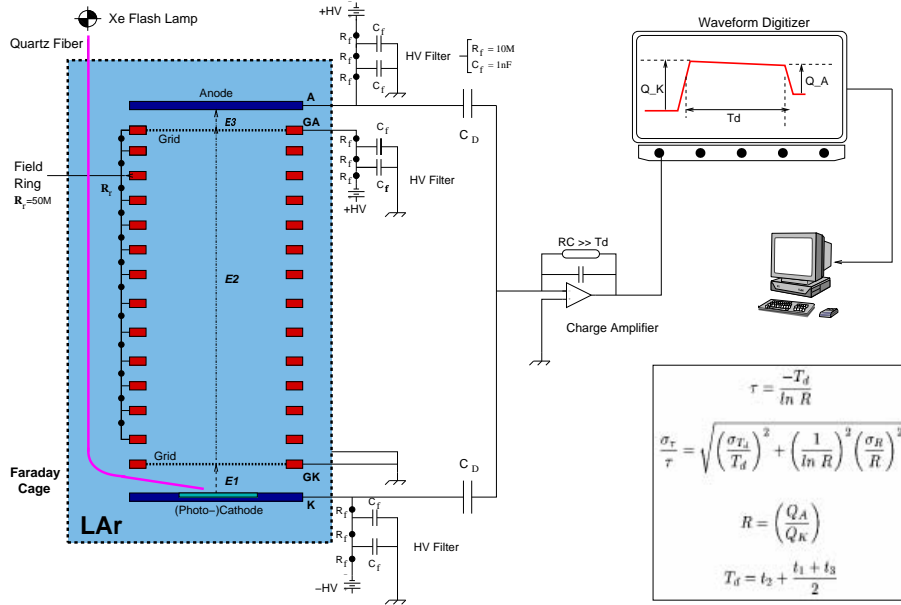


Figure 1: Layout of the PrM unit and read-out scheme.

PrM mechanical structure	stainless steel
K, A Disk diameter	80 mm
K- A total drift distance	188 mm
K- GK gap	18 mm
GK- GA gap	160 mm
GA- A gap	10 mm
Number of Field shaping rings	15
Field shaping ring Diameter/Pitch	80 mm , 10 mm
Grids (GK, GA)	BMC MN-73 (Nikel Mesh)
Grid diameter	60 mm
Grid inter-wire spacing	1.9 mm
Grid wire diameter	0.1 mm
PrM Optical fibre	
Type/Material	FORT HGC-M0940T, Quartz (all silica)
Diameter	940 μ m
inclination	20°
attenuation	1db/m @ $\lambda = 95$ nm
Photo-Cathode: PrM Id. #.	Material
# 1 _A , # 2 _A	Metal (Gold deposit on Brass)
# 4 _A	Semiconductor (CdZnTe)
# 3 _A , # 5 _A , # 6 _A	Semiconductor (GaAs)

Table 1: Geometrical characteristics of the Purity Monitor

The two grids are electro-formed Nickel meshes, with 1.9 mm wire spacing, 100 μm wire diameter and 89.7% geometrical transparency. The flatness of the grid plane is guaranteed by a mesh holder formed by two rings pinching the mesh in between.

A mechanical structure, formed by a system of vetronite threaded rods, spacers and bolts, holds together the electrodes. Both materials, stainless steel and vetronite, have similar thermal coefficient, to guarantee negligible thermal stresses during cool-down operations. The mechanical stability of the device results to be extremely satisfactory and suitably matching the requirement of long operation in cryogenics environment.

HV potential can be applied independently from a multi-channels HV supply to the K, GK, GA, A electrodes by electrical connections to the corresponding pins of a vacuum tight feed-through mounted on one of the exit flanges of the cryostat. Inside the cryostat four coaxial cables are employed, whose shieldings are soldered together and connected to an independent pin of the feed-through for the ground connection. The length of the cables (from 5 m to 8 m) is determined by the position of the PrM inside the LAr vessel.

The grids and the field-shaping rings are connected by a high-value resistor chain (50 $\text{M}\Omega$ each), so to realize a resistive divider for the electric potential applied between the two grids. This scheme ensures the uniformity of the electric fields (E_1, E_2, E_3) in the three drift regions (between K-GK, GK-GA and GA-A respectively). Typical field values, according to $E_3 > 2E_2 > 2E_1$ proportions (see Sec. 3.1.1 and Eq. (3) therein), range between few tens of V/cm in the first gap and some hundreds of V/cm in the other gaps. The grid geometry combined with the HV bias applied to the electrodes guarantees maximum transparency (i.e. the minimum number of drifting electrons lost crossing a grid) and maximum shielding (drift of the electrons before a grid does not affect the field after the grid), see Fig. 2.

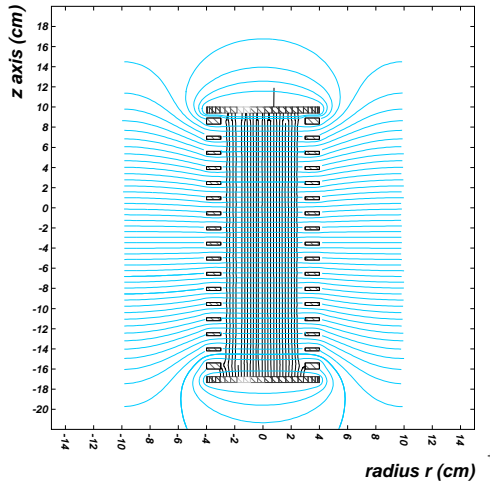


Figure 2: *Electric field lines and equi-potential contours in the PrM cross-section plane.*

Each PrM is contained in a stainless steel pierced Faraday cage to isolate the system from/to the outside electrostatic interference. After installation in the LAr vessel of the T600, the cage is mechanically and electrically connected to the stainless steel frame of the

wire chamber.

We adopted two electrical connection schemes for the HV biasing of the PrM. The first scheme allows to drive independently the high voltage of the four electrodes (K, GK, GA, A). With the second electrical scheme, shown in Fig. 1, the cathode-grid (GK) is referred to ground via electrical connection to the Faraday cage and through it to the general ground of the cryostat. From preliminary tests performed before installation this layout has shown some advantages in terms of noise compared to the other scheme, and therefore it has been adopted for four of the six monitors installed in the first half-module of the T600 detector.

3.1.1 Grid transparency

The electrical transparency of a grid is a function of the ratio of the fields E_1, E_2 before and after the grid respectively, and of the geometrical ratio $\rho = 2\pi r/s$, where r is the radius of the mesh wire and s is the inter-wire spacing (values of r and s for the mesh used in our PrM units can be found in Tab. 1).

According to theory [5, 6, 1] the grid is 100% transparent if:

$$\frac{E_2}{E_1} > \frac{1 + \rho}{1 - \rho} \simeq 2 \quad ; \quad \rho = \frac{2\pi r}{s} = 0.33 \quad (3)$$

Therefore, the electric field values in the three gaps of the PrM unit have to be set according to $E_3 > 2E_2 > 2E_1$ proportions to obtain full transparency.

The shielding inefficiency σ is defined as the fraction of field change in E_1 due to E_2 . This is given by:

$$\sigma = \frac{dE_1}{dE_2} = \frac{s}{2\pi d_1} \log\left(\frac{s}{2\pi r}\right) = 1.9\% \quad (4)$$

where d_1 is, for example, the K-GK distance.

Note that σ is a function of geometry only, and does not depend on the applied fields. Note also that these considerations apply fully to a wire mesh of circular section. In the PrM units the grid is made out of an electroformed mesh and the mesh wires have a rectangular cross section. Taking Eq. 4 as approximate, and dealing with the geometrical characteristics of the employed mesh, we obtain a shielding inefficiency of about 2%.

3.2 Photo-cathode and light source

The photo-cathode is the most important component of the PrM unit. The precision on the lifetime determination depends on the actual signal-to-noise conditions provided by the system, the signal being the charge amplitude extracted from the cathode and subsequently collected by the anode. In the first T600 half-module four PrM units are equipped with elemental semiconductor (GaAs and Cd(Zn)Te) photo-cathode and two with metal (Au) photo-cathode.

In recent years there was a growing interest in developing electron sources based on semiconductor photo-cathode, able to produce much larger charge yield than metal-based photo-cathodes, thanks to the combined effect of their (typically) higher quantum efficiency (QE) and lower surface barrier. In metals, QE is limited by (1) the low photon-to-electron conversion efficiency, due to their high optical reflectivity, and (2) the charge loss due to electron-electron scattering during their motion in the solid from the production point to the surface. Typical QE values are in the range of $10^{-5}\%$ - $10^{-4}\%$ electrons per incident

photon. The surface barrier in metals is typically high, being determined by the Work function of the order of ≤ 3 eV, corresponding to photon wavelength ≤ 400 nm (i.e. in the UV region). In semiconductors (SC) the QE value can be large, for photons with energy greater than the SC energy gap (E_g), due to the limited charge loss dominated by electron-phonon scattering in the solid. Moreover, the surface barrier can be low, being determined by the SC electron affinity (E_A) and by the energy gap: $E_g + E_A > 2eV$ for many SC types formed by compounds of alkaline elements (opening the possibility to employ visible light for photo-extraction). The combined effect results in QE values for SC in the range of $10^{-4}\%$ - $10^{-1}\%$ electrons per incident photon.

Particular mention should be deserved to those particular photo-cathodes, usually called *NEA* (Negative Electron Affinity) photo-cathode, obtained by deposition of thin alkaline metal layer on SC surface. In this case a band bending effect may take place, reducing the photo-electric threshold and increasing the QE to macroscopic values, up to the 10% level in the visible light spectrum. Vast applications of NEA materials is found as photo-emitters in photomultiplier technology.

In spite of the promising properties of SC, their use as photo-cathodes in our PrM systems is practically prevented by the chemical reactivity shown by the SC with alkaline elements¹ and by the NEA emitters. The oxidation of the surface during the exposure to atmosphere, before deployment in LAr, turn into a large degradation of the QE value.

All elemental SC with stable chemical characteristics, like Si, GaAs, CdTe, have higher surface barrier (4 to 6 MeV), therefore requiring the use of adequate UV photon source. Their QE is in general higher than metals, at least one order of magnitude better. This is the motivation of the adopted choice of equipping the PrM with elemental SC photo-cathodes.

A first, dedicated set of measurements have been pursued by our group, aiming to the characterization of a number of SC samples of various types [7]. The tested samples were of metals (Au, brass, Cu) and of semiconductors (GaAs, CdZn, InSb, etc.) with different levels and types of doping). All the tested materials emit only under UV radiation. Some SC have photo-electron yields significantly higher than metals. The best results in term of QE have been shown by GaAs and Cd(Zn)Te.

This lead to the choice of equipping the PrM for the first T600 half-module with these types of SC as photo-cathode material. A second set of tests is on-going. Samples of Si, p-type doped, show even larger QE when microstructured surfaces are realized (porous surface by electrolytic method). The R&D programme is still active, with the promising study of the field assisted photo-emission from different Si microstructured surfaces (pores, micropores, microtips and nanotubes).

All materials investigated so far, and compatible for the particular application as photo-cathodes for the PrM system, show photo-emission under UV light, with wavelength below about 300 nm. This implies the use of suitable UV light sources and UV light transport means (from the source to the photo-cathode).

A quartz optical fibre (~ 1 mm core diameter, all silica) allows to drive the light (down to 180 nm of wavelength) from the source, outside the vessel, onto the photo-cathode. A fibre holder, realized in Peek and mounted on the cathode disk, keeps the fibre-end in place at a distance of 2 mm to the cathode centre and at an angle of 20° to the cathode plane.

¹A dedicated test has been performed at LNGS: a thin layer of alkaline material (Mg) has been deposited by sputtering on a semiconductor photo-cathode. A very large increase in quantum efficiency has been found. However, a fast degradation has been noted as soon as the photo-cathode has been exposed to atmosphere.

A cryogenics, Indium sealed feed-through allows the fibre to exit the LAr vessel without break up to the light source at the other end. The length of the fibre (from 4 m to 7 m) is determined by the position of the PrM inside the LAr vessel.

The main geometrical parameters and characteristics of the device are listed in Tab. 1; details of the PrM structure are shown in Fig. 3;

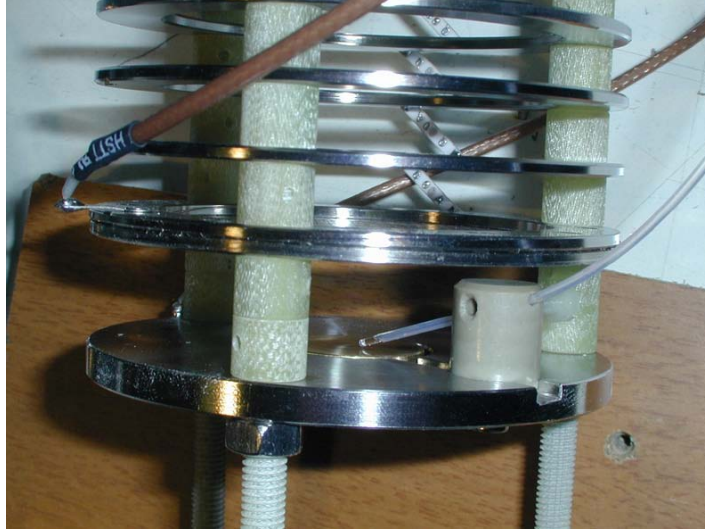


Figure 3: *Details of the purity monitor structure.*

The choice of the best suited UV light source is fundamental: the light must be fed in pulsed mode, with high pulse energy and short duration. The adopted solution consists in a commercially available pulsed Xenon (Xe) flash lamps. The pulse width is of few μs , with wavelength spectrum ranging from $\lambda \sim 185 \text{ nm}$ to $\sim 2000 \text{ nm}$. The emission peak is located around $\lambda \sim 240 \text{ nm}$ ($\sim 4.9 \text{ eV}$). The lamp bulb is housed in a portable container together with two biconvex fused silica lenses focusing the UV light onto the the optical fibre-end. This system (Xe lamp + lenses + micrometric adjuster for the fibre) is an easy handling, portable device well suited for its application in routine lifetime measurements.

3.3 Read-out system

When the PrM is immersed in LAr and a short UV light pulse generated by the Xe lamp impinges on the photo-cathode the photo-extracted electron bunch drifts toward the first grid, inducing a current on the cathode during the time interval t_1 . After crossing GK, the electron bunch drifts along the distance between the grids. During this time (t_2), no current is induced on K or A, due to the shielding effect of the grids. After, a current flows through the anode during the time t_3 when the electrons move toward A after crossing GA. The extension of each time interval depends on the strength of the electric field in the corresponding gap. A charge amplifier allows to measure the charge Q_K and Q_A from integration of the anode and cathode signals in t_1 and t_2 respectively. The current is approximately constant, assuming that the lamp pulse width is short compared to the time interval.

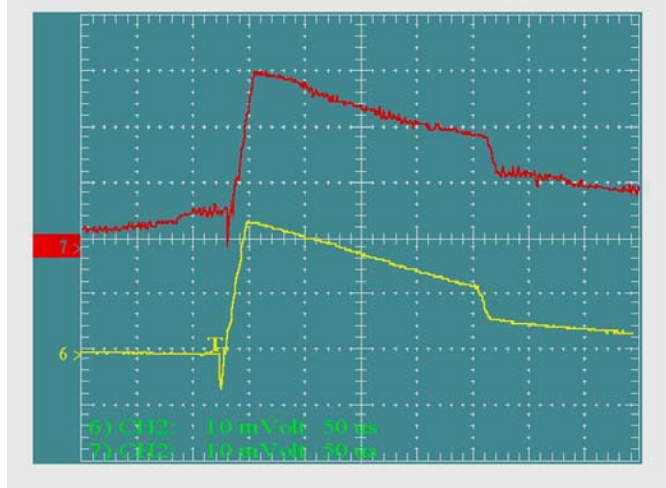


Figure 4: *Typical PrM waveforms: [Top] single Xe lamp shot, [Bottom] averaged over several shots*

A compact, dedicated system has been designed for the read-out and storing of the charge information from each PrM unit [8]. It is composed by (1) a Decoupling Stage formed by a HV filter and a pick-up capacitor (C_D), (2) a single Charge Amplifier and (3) a Waveform Digitizer, see Fig. 1. An aluminum cylindrical case, mounted directly on the electrical feed-through (outer side), hosts the Decoupling Stage as well as the charge Amplifier (AMPTEK - A250). On the top flange of the case there are the input HV and output signal connectors. This setup minimizes ambient noise pick-up and the amplifier input capacitance due to the signal cable length. Both anode and cathode signals feed the input stage of the amplifier (AC coupling), so to avoid the necessity of an inter-calibration of two signal amplitudes. The current signals from the anode and from the cathode are opposite in sign. Therefore, the charge amplifier output signal results in a trapezoidal waveform as a function of time, whose three main features (rising edge, flat top, falling edge) correspond to the three drifting gaps of the purity monitor. As indicated in Fig. 1, the amplified signal is carried to a digital scope, where the digitized waveform is stored for the electron lifetime estimation. The scope is read-out by a PC mounted in CompactPCI frame, via an ethernet link. Waveforms and lifetime values obtained by waveform analysis are stored on a MySQL database (during the test run of the first T600 half-module the read-out was performed manually on the scope).

3.4 Lifetime determination

Waveforms recorded with PrM #3_A during the Pavia test run are shown in Fig. 4. The measurement of the rise and fall amplitudes (corresponding to Q_K and Q_A), along with the pulse duration (the drift time T_d) gives a direct estimation of τ_e at the time of the measurement [4].

Let Q_0 be the charge extracted from K by the light pulse at the time $t = 0$. Let the electric fields be (E_1, E_2, E_3) [V/cm] in the three drift regions (between K-GK, GK-GA and GA-A respectively). The corresponding drift velocities in the three gaps are v_1, v_2, v_3 (where

$v_i = \alpha E_i + \beta E_i^2$ [mm/ μ s] - $\alpha = 0.57E-2$, $\beta = -0.72E-5$, as obtained by a P2-polynomial fit of experimental data at low fields²) and t_1, t_2, t_3 the corresponding drift times. The pulse duration is assumed to be negligible with respect to the drift time of the electrons in the first gap of the PrM chamber.

The charge amplitude Q_0 depends on the strength of the electric field E_1 (when no electric field is applied most of the charge is instantly re-absorbed on the cathode due to the presence of the LAr dielectric medium). Measurements of extracted charge as a function of the electric field strength E_1 (i.e. in the K-GK gap) have been performed. The behavior of the extracted charge turns out to be well represented by a logarithmic function of the field. In Fig. 5 the extracted charge Q_0 as a function of E_1 is shown as well as the fitting function (Q_0 values have been corrected for the effect of the measured finite lifetime of the liquid during the measurement).

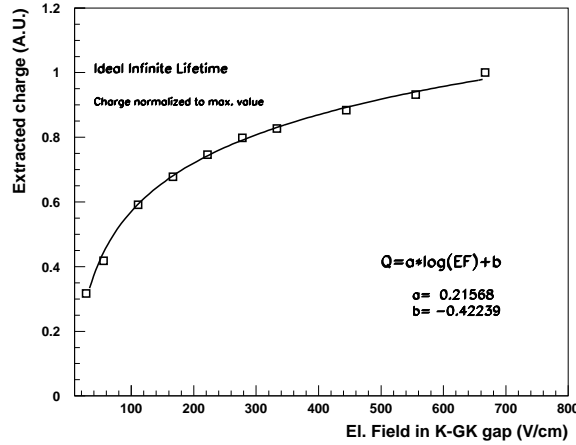


Figure 5: *Extracted charge Q_0 as a function of the electric field in the K-GK gap. Continuous line refers to a logarithmic fit of data.*

In an ideal case, when no electro-negative impurities are present in the liquid (infinite lifetime), a current I_K (I_A) constant in time is induced on K (A) during the time interval $[0, t_1]$ ($[t_1 + t_2, t_1 + t_2 + t_3]$):

$$I_{K,A} = \frac{Q_0}{d_{1,3}} v_{1,3} \quad (5)$$

In the real case (finite τ_e value) the current is progressively attenuated with time:

$$I_{K,A}^{att}(t) = \frac{Q_0}{d_{1,3}} v_{1,3} e^{-\frac{t}{\tau}} \quad (6)$$

Since electrons move away from K and against A, the two currents I_K and I_A are opposite in sign (see Fig. 6 [Top]). Now, let Q_K and Q_A be the charge amplitude at the cathode

²The drift velocity depends on the actual value of the LAr temperature. The P2-fit has been performed with data corresponding to a temperature of 89K.

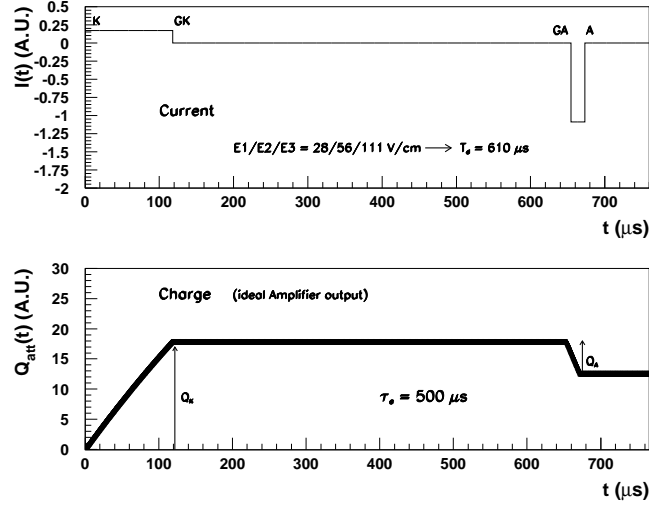


Figure 6: [Top] Current Waveform, [Bottom] Charge Waveform from analytical calculation

and at the anode, respectively. Integrating in the gap between K and GK, for a given value of τ_e we obtain:

$$Q_K^{att} = \int_0^{t_1} I_K^{att} dt = \frac{Q_0}{t_1} \tau (1 - e^{-\frac{t_1}{\tau}}) \quad (7)$$

Integrating in the third gap, between GA and A, we obtain:

$$Q_A^{att} = \int_{t_1+t_2}^{t_1+t_2+t_3} I_A^{att} dt = \frac{Q_0}{t_3} \tau e^{-\frac{t_1+t_2+t_3}{\tau}} (e^{\frac{t_3}{\tau}} - 1) \quad (8)$$

In Fig. 6 the Current signal waveform [Top] and the corresponding Charge signal waveform [Bottom], as obtained by an analytical calculation ($\tau_e = 500\mu s$) are shown. The difference between the two Charge waveforms, from analytical calculation (Fig. 6 [Bottom]) and from experimental measurement (Fig. 4), is mainly due to the presence of the Charge Amplifier, with its characteristics of rise-time and decay-time, not included in the analytical calculation.

The ratio R between the two charge amplitudes is:

$$R = \frac{Q_A}{Q_K} = \frac{t_1}{t_3} \frac{e^{\frac{t_3}{\tau}} - 1}{1 - e^{-\frac{t_1}{\tau}}} e^{-(\frac{t_1+t_3}{2}+t_2)} \quad (9)$$

With some algebra, it can be re-written as:

$$R = \frac{t_1}{t_3} \frac{\sinh(\frac{t_3}{2\tau})}{\sinh(\frac{t_1}{2\tau})} e^{-(\frac{t_1+t_3}{2}+t_2)} \quad (10)$$

If t_1 and t_3 are small with respect to t_2 , the term in square brackets can be considered as unity and the electron lifetime can be calculated as:

$$\tau_e = \frac{1}{\ln(R)} \left(t_2 + \frac{t_1 + t_3}{2} \right) = \frac{-T_d}{\ln(R)} \quad (11)$$

where T_d defines the actual “drift time” of the electron bunch inside the PrM drift volume.

3.4.1 Error on Lifetime determination

The ratio $R = Q_A/Q_K$ is strongly related to the LAr purity. When the ratio results to be close to its boundary limits ($R \rightarrow 1$ for very good purity and $R \rightarrow 0$ for bad purity of the liquid) the actual value of τ_e is intrinsically determined with poor accuracy. This is shown by the error calculation leading to the following expression:

$$\frac{\sigma_\tau}{\tau} = \sqrt{\left(\frac{\sigma_{T_d}}{T_d}\right)^2 + \left(\frac{1}{\ln R}\right)^2 \left(\frac{\sigma_R}{R}\right)^2} \quad (12)$$

The relative error on the drift time determination (first term in the r.h.s of Eq. (12)) is rather small. From experimental measurements we assume it as a constant term:

$$\frac{\sigma_{T_d}}{T_d} = 3\% \quad (13)$$

Fluctuations on the electron charge Q_0 initially extracted and electronics noise, both affecting the signal amplitude (Q_A and Q_K , see Eqq. (8)(7), in the ratio R , Eq. (10)) also limit the precision on the determination of the lifetime, particularly for low τ_e values:

$$\frac{\sigma_R}{R} = \sqrt{\frac{\sigma_{Q_A}^2}{Q_A^2} + \frac{\sigma_{Q_K}^2}{Q_K^2}} \quad (14)$$

We assume that the relative error on the measured charge amplitudes can be parametrized with the following expression:

$$\frac{\sigma_Q}{Q} = \sqrt{\frac{k^2}{Q} + \frac{h^2}{Q^2}} \quad ; \quad Q = Q_A, Q_K \quad (15)$$

The first term is a “Poisson term” due to the stochastic nature of the extraction mechanism, while the second one is an “electronic noise term”. The characteristic parameters k and h have been determined experimentally during the PrM test phase ($k = 10\%$ and $h = 0.3$ expressed in mV). The choice of one of the most sophisticated low noise/high gain amplifiers available aimed at limiting as much as possible this source of systematic error.

One should also note from Eq. (15) that the relative error on the charge amplitude increases when the extracted charge Q_0 is smaller (both Q_A and Q_K depend on the actual value of the extracted charge according to Eqq. (8), (7)). This happens when a low electric field is applied in the K-GK gap, see Fig. 5. This turns out to be the most limiting factor for a precise determination of the lifetime. To increase the amount of extracted charge, the design of the PrM system, as described in the previous sections, has been extensively upgraded: from the choice of the most powerful Xe lamps available to the selection of large

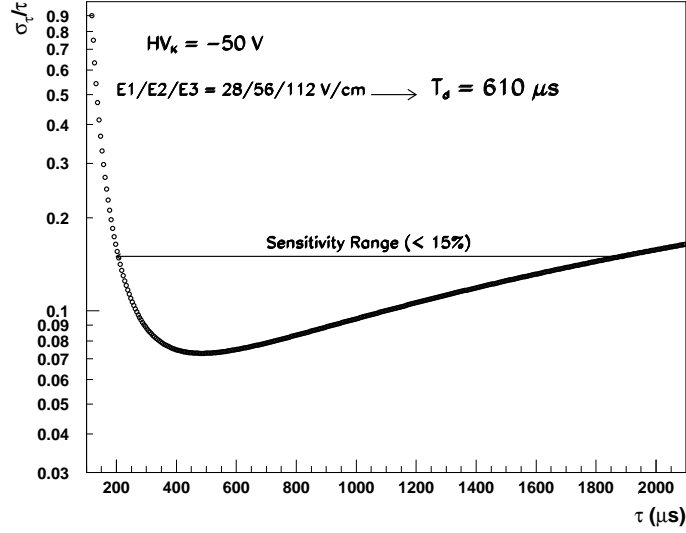


Figure 7: Expected error (%) on τ_e and sensitivity range for long T_d configuration.

core UV fibres (aiming both to increase the amount of light impinging on the photo-cathode), from the search for suitable high quantum efficiency photo-cathodes to the careful design of the HV system (shielding, cables, feed-through) allowing electrodes biasing at high voltage (aiming both to increase the amount of electrons extracted and subsequently drifting inside the PrM chamber³).

The range of *sensitivity* (i.e. where τ_e is measured by our PrM unit with a given precision) can be tuned according to the extension of the drift time chosen by appropriate HV biasing of the electrodes. Within some limits, sensitivity to high (low) values of τ_e is obtained for longer (shorter) values of T_d . As an example, tuning the HV biasing of the electrodes in order to ensure maximum transparency ($E_3 > 2E_2 > 2E_1$) and to have an electron drift time of the order of few hundreds microseconds ($E_1 = 28\text{V/cm}$, $E_2 = 56\text{V/cm}$ and $E_3 = 112\text{V/cm}$ with a corresponding value of $T_d = 610\mu\text{s}$) we estimate from Eq. (12) to (15) that the lifetime measurement can be carried out with a satisfactory systematic precision of $\mathcal{O}(\leq 15\%)$, for lifetime values within $200\mu\text{s} \leq \tau_e \leq 2\text{ms}$ (see Fig. 7).

To have a more general overview of the sensitivity of the PrM system we have calculated the *iso-sensitivity contours* in the plane τ_e vs HV_K applied on the cathode. Assuming, as in our preferred scheme, to have GK connected to ground, at each value of HV_K corresponds a defined choice of the HV bias of the other electrodes to obtain maximum transparency (i.e. HV_K is the only free parameter to be set). This allows us to calculate σ_τ/τ , Eq. (12), as a

³During the T600 test, with a medium power Xe lamp, the extracted charge was measured to be corresponding to a signal of about $Q_0 = 20\text{mV}$ (for $HV_K = -50\text{V} \rightarrow E_1 = 28\text{V/cm}$) at the output of the charge amplifier. This value has been used as absolute normalization value of the extracted charge (Fig. 5) for the calculations reported in this section.

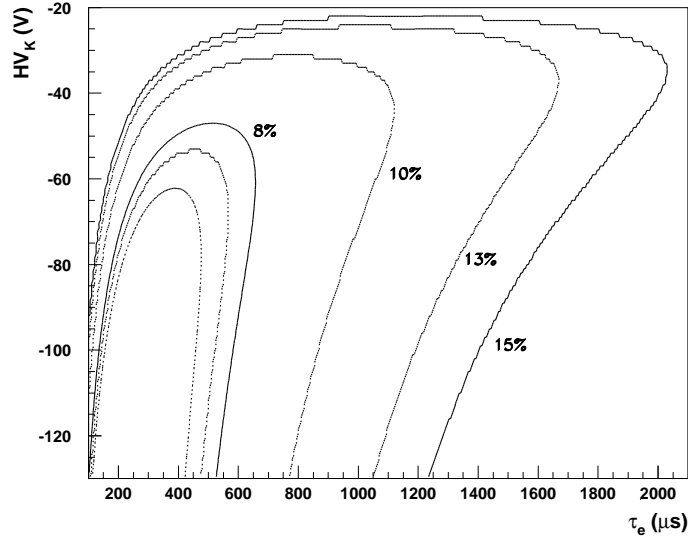


Figure 8: *Iso-sensitivity contours in the lifetime vs HV_K plane.*

function of τ_e for any HV_K choice. Contours of *iso-sensitivity*, reported in Fig. 8, are defined for various level of precision. In conclusion, the outer contour defines the region where the electron lifetime measurements can be performed with a satisfactory systematic precision of $\mathcal{O}(\leq 15\%)$.

3.5 Installation in the T600 detector

The two T600 half-modules have been equipped with six PrM units each, located outside the LAr imaging volume at different heights, see Tab. 2 and Fig. 9. In Fig. 10 two fully mounted PrM units of the first half-module are shown before (after) insertion in the electrostatic cage.

Before installation each unit was individually cleaned and tested (1) in vacuum, (2) in Argon gas and (3) in LAr with a dedicated cryogenics facility LACF at LNGS. The test aimed to check the correct functionality of the monitor and to obtain a cross reference list of the working parameters.

After installation inside the T600 half-modules cables and optical fibre of each PrM unit have been connected to a corresponding pair of electric and optical feed-throughs. Three large CF-200 flanges located on the top of each T300 cryostats have been used for the connection with the outside world. Each flange embeds four apertures terminated with CF-40 flanges for two pairs of electric and optical feed-throughs. In this way each large flange hosts the connection of two of PrM-units. In Fig. 11 one fully equipped flange is shown.

During the Pavia test the six PrM units of the first half-module have been individually tested. All of them were properly working. Only PrM #3_A was routinely used for the

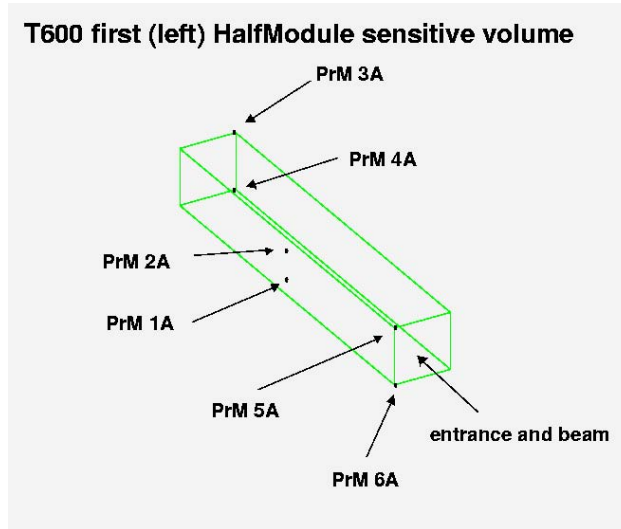


Figure 9: *Positions of the PrM units inside the first T600 half-module.*

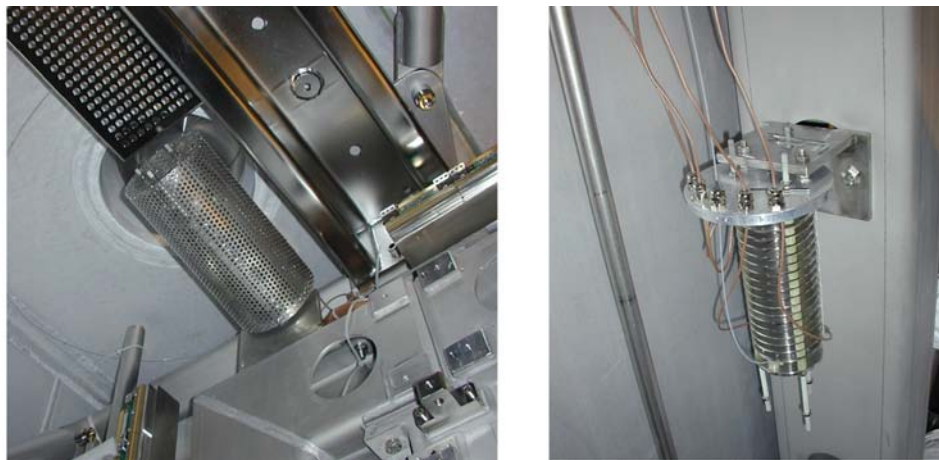


Figure 10: *Purity monitors after mounting in the T600 (1st half-module) detector: [Left] PrM#3_A in final configuration (inside Faraday cage), [Right] PrM# 2_A before insertion in the Faraday cage.*



Figure 11: *Positions of the PrM units inside the first T600 half-module*

PrM Id.#	height from cryostat bottom
# 1 _A	1250 mm
# 2 _A	2475 mm
# 3 _A	3660 mm
# 4 _A	285 mm
# 5 _A	3660 mm
# 6 _A	285 mm

Table 2: *Height from cryostat bottom of the T600 purity monitors (first half-module).*

reference measurement of the LAr purity during the three months of the Pavia test. The set of measurements provided a precise indication of the lifetime evolution during the test run. This result is reported in [9] and turns out to be in very good agreement with the lifetime estimation from the calorimetric analysis of muon tracks crossing the LAr imaging volume.

References

- [1] The ICARUS Collaboration, “ICARUS I: an optimized, real time detector of solar neutrinos”, **LNF-89/005** (1989), Sec.2.
- [2] G. Carugno et al. (The ICARUS Collaboration), “Electron lifetime detector for liquid Argon”, *Nucl. Instr. and Meth. A* **292** (1990), 580.
- [3] “Improved Electron lifetime monitor for ICARUS T600”, **ICARUS-TM/98-04** (1998).
- [4] A. Bettini et al. (The ICARUS Collaboration), “A study of the factors affecting the electron lifetime in ultra-pure liquid Argon”, *Nucl. Instr. and Meth. A* **305** (1991), 177.
- [5] E.Gatti et al., *IEEE Trans. Nucl. Sci.* **NS-26**, **2** (1979), 2910.
- [6] E. Buckley et al.(The ICARUS Collaboration), *Nucl. Instr. and Meth. A* **275** (1989), 364.
- [7] F. Arneodo et al., “Electron Beam generation from semiconductor photo-cathodes”, *Rev. Sc. Instr.* **Vol.72**, **n.1** (2001), 63.
- [8] “General Layout of the Purity Monitoring System of the ICARUS T600 detector at LNGS”, **ICARUS-TM/02-15** (2002).
- [9] The ICARUS Collaboration, “Study of the electron lifetime with the ICARUS detector (Pavia test run)”, paper in preparation (2002).